Late Archean euxinic conditions before the rise of atmospheric oxygen

C. Scott, A. Bekker, C. T. Reinhard, B. Schnetger, B. Krapež, D. Rumble III and T. W. Lyons

Geological and depositional setting of studied samples

The Marra Mamba Iron Formation is the stratigraphically lowest iron formation of the Hamersley Province in Western Australia. It is interpreted to have been deposited in a deep-water setting on a passive margin (Krapež et al., 2003). The underlying succession comprises, in descending order, the Roy Hill Shale, the Warrie Member, the Woodiana Sandstone (collectively making up the Jeerinah Formation), and the Maddina Basalt. The Maddina Basalt, Woodiana Sandstone and the Warrie Member together record the last stage of a protracted rifting event that opened an ocean to the south (Blake and Barley, 1992). The Roy Hill Shale records a rift-drift transition and its basal contact is a breakup surface. At most localities the contact between the Warrie Member and the Roy Hill Shale is conformable, but in some cases the contact is a subaerial erosion surface. The Roy Hill Shale is conformable with the overlying Nammuldi Member, which is the lowermost division of the Marra Mamba Iron Formation. The age of the Jeerinah Formation is defined by a 2,662 ± 7 Ma U-Pb zircon age from a thin, <1 mm-thick, ash-fall tuff at the top of the Roy Hill Shale Member, the upper Jeerinah Formation (Rasmussen and Fletcher, 2010).

FVG-1 was drilled between 1983 and 1984 by CRA Exploration Pty Ltd. in the Fortescue Valley between the North Pilbara Granite-Greenstone Terrain to the north, and the Hamersley Province to the south at 22º 33'S, 119º 30'E. The drill-hole section, comprising the Nammuldi Member, Roy Hill Shale, Warrie Member, Woodiana Sandstone and Maddina Basalt, is typical of those successions, but most of the Marra Mamba Iron Formation is faulted out. The distinction in drill-core between the Warrie Member, Roy Hill Shale and Nammuldi Member is easily made. The Warrie Member comprises thin bedded carbonate turbidites and organic matter-rich (black) shales, but the shales lack abundant early diagenetic pyrite. The Roy Hill Shale consists of organic matter-rich (black) shale with abundant early diagenetic pyrite. The Nummuldi Member consists of stilpnomelane-rich shales and thin-bedded carbonate turbidites but contains little early diagenetic pyrite. The drill-hole also contains a meteorite-impact spherule bed (at drill-depth 750.68 m) that has now been recognized in many drill-hole sections throughout the Pilbara region of Western Australia and also in South Africa (Simonson et al., 2000).

The Hamersley Province, the site of deposition for the Jeerinah Formation, is mildly deformed and metamorphosed, with depth of burial being the primary control on metamorphic grade (Smith et al., 1982). The FVG-1 drill-hole was drilled in the area that experienced prehnite-pumpellyite-epidote facies of metamorphism.

Archaean Sulfur Budget

Presence of large MIF in S isotopes suggests that photochemically-processed and volcanically-derived SO_2 was the main sulfur source for pyrite in shales of the Jeerinah Formation. We envision, based on the range of MIF in pyrites, that volcanic emissions with SO_2:H_2S ratios ranging between 2 and 10 delivered sulfur to the ca. 2.66 Ga anoxic atmosphere (cf. Halevy et al., 2010). SO_2 was photolyzed in the oxygen- and ozone-free atmosphere and sulfate and elemental sulfur aerosols carried sulfur with MIF to the ocean (cf. Farquhar et al., 2001; Pavlov and Kasting, 2002; Zahnle et al., 2006). Hydrogen sulfide and sulfur dioxide that escaped photolysis in the atmosphere did not carry MIF and therefore diluted MIF in sulfur compounds delivered from the atmosphere. We develop below a simple mass-balance model to account for sulfur concentrations in shales of the Jeerinah Formation using volcanic sulfur as the single sulfur flux to the Archean anoxic atmosphere-ocean and reasonable sedimentation rates for deposition of organic matter-rich shales.

Estimates of the modern volcanic SO_2 flux range widely, from values of 1.5×10^{12} g SO_2/yr[14] to those approaching 50×10^{12} g SO_2/yr (Lambert et al., 1988). However, recent extensive compilations that integrated flux measurements on relatively long timescales yield estimates of ~15-20 $\times 10^{12}$ g SO_2/yr (Berresheim and Jaeschke, 1983; Bluth et al., 1993; Andres and Kasgnoc, 1998; Halmer et al., 2002). Although the bulk of the modern volcanic sulfur flux is typically considered to be in the form of SO_2, the flux of H_2S from volcanoes is poorly constrained and has been estimated to be as high as 37×10^{12} gH_2S/yr (Halmer et al, 2002).

Assuming an SO_2 outgassing rate of 15×10^{12} g SO_2/yr and a conservative H_2S outgassing rate of 3×10^{12} g H_2S/yr yields a total sulfur outgassing rate of 1.8×10^{13} g S/yr. We adopt this as our minimum modern flux rate and assume a value of 3.2×10^{13} g S/yr as our maximum modern flux (Holland, 2002). Assuming that roughly half of this is mantle sulfur (e.g., Habicht et al., 2002), we obtain a modern mantle flux of between 9.0×10^{12} and 1.60×10^{13} g S/yr. Rather than making assumptions regarding the areal extents of continents versus oceans during the Archean, we integrate this flux over the entire surface of the Earth to yield a globally averaged mass flux of $1.77 – 3.14 \times 10^{-2}$ g/m^{2}yr for volcanic sulfur of mantle origin given modern outgassing rates.

For a sediment accumulating at ~1 m/Myr (a reasonable post-compaction accumulation rate for a distal black shale (Leventhal, 1991; Schieber and Baird, 2001; Schieber, 2009), assuming a typical shale density of 2.7 g/cm^3, this globally averaged mass flux would correspond to the accumulation of 0.65 – 1.16 wt% pyrite sulfur, slightly lower than the average pyrite sulfur content of the euxinic Roy Hill Member (2.41±1.09 wt%). If we assume that the bulk of this

mantle sulfur flux was sequestered as pyrite in depositional environments similar to those represented by the Roy Hill Member (i.e., ~2.41 wt% pyrite sulfur accumulating at ~1 m/Myr), then the areal extent of this depositional mode could have been ~22 – 68% of the modern seafloor area.

The upper end of this range is probably extreme, as it is not likely that the entire inventory of volcanic sulfur would be sequestered in a single depositional facies. Additionally, bulk sediment accumulation rates may have been somewhat faster than our assumed post-compaction rate of 1 m/Myr, which would result in lower calculated pyrite sulfur concentrations and a more restricted areal extent of sulfidic deposition. For example, doubling the accumulation rate to 2 m/Myr would yield a range of 0.19 – 0.58 wt% pyrite sulfur and an areal extent of 11 – 34% of the modern seafloor, using the same mantle flux. On the other hand, Archean outgassing rates were probably elevated relative to the modern (Kasting, et al., 1989; Zahnle et al., 2006), which would presumably have resulted in a commensurate increase in volcanic SO_2 and H_2S fluxes, and, regardless of the mode of subduction assumed for this period of Earth's history, it seems likely that some sulfur of sedimentary origin would have contributed to the overall volcanic flux. These calculations also neglect contributions from other gases such as CS_2 and OCS, whose combined modern flux may be as high as ~2.5 x 10^{11} g S/yr (Halmer et al., 2002), and direct emissions of SO_4^{2-} in volcanic plumes, which may be significant (Berresheim and Jaeschke, 1983). These vagaries aside, it seems clear that even a modest volcanic sulfur source could have provided for the sulfur burial flux recorded by the Roy Hill Shale, resulting in potentially widespread euxinic deposition given variations in the availability of organic carbon, Fe_{HR}, and volcanic activity.

Iron Speciation

Although ferruginous deposition for the lower Roy Hill Member is clearly indicated by the combination of elevated Fe_T/Al ratios and low values for Fe_{PY}/Fe_{HR}, these samples also display the unusual combination of high Fe_T/Al ratios and relatively low Fe_{HR}/Fe_T values. Although this relationship could result from authigenic and/or metamorphic formation of Fe-containing silicate mineralogies, it is also possible that the extraction of Fe_{HR} is incomplete for samples with high concentrations of crystalline or coated siderite, a phenomenon suggested by Reinhard et al. (2009) for the Mt. McRae Shale. To test this possibility, we performed an additional, aggressive boiling HCl extraction (Fe_{HCl}), which quantitatively mobilizes all siderite and all other Fe_{HR} phases, as well as any authigenic Fe silicate minerals and some amount of poorly reactive silicate phases. Samples from the Roy Hill Member show a reasonably good correspondence between sequentially extracted Fe_{HR} content and Fe_{HCl} content, with the exception of some samples from the lower ferruginous interval (Fig. DR1). We interpret this inconsistency to reflect an underestimation during the sequential procedure of Fe_{HR} present as

refractory siderite and/or secondary sili cates. We e mphasize that this additional Fe_{HR} would increase Fe_{HR}/Fe_T ratios while decreasing Fe_{PY}/Fe_{HR} values, thereby strengthening our argum ent for an Fe(II)-containing water column prior to the onset of euxinia.

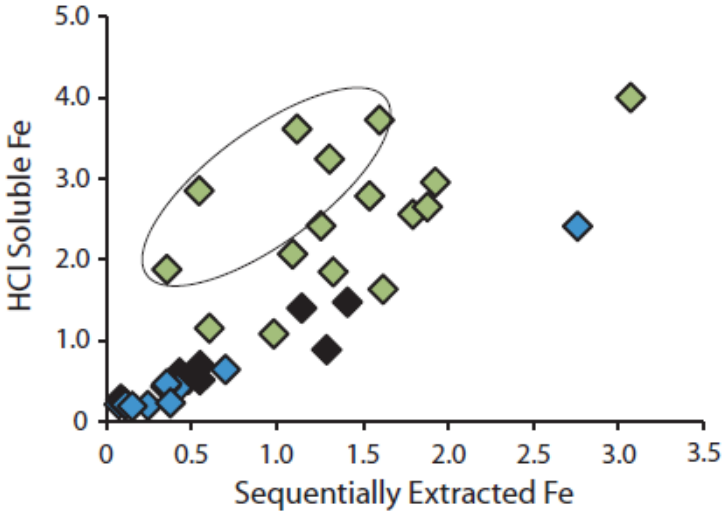

Figure DR1. Cross-plot of HCl soluble Fe and sequentially extracted Fe for the Jeerinah Formation. Blue diamonds: euxinic interval; black diamonds: upper ferruginous interval; green diamonds: lower ferruginous interval. Open field encompasses samples where Fe_{HR} is underestimated by the sequential extraction

References Cited

Andres, R.J., and Kasgnoc, A.D., 1998, A time-averaged inventory of subaerial volcanic sulfur emissions: Journal of Geophysical Research, v. 103, p. 25251-25261.

Berresheim, H., and Jaeschke, W., 1983, The contribution of volcanoes to the global atmospheric budget: Journal of Geophysical Research, v. 88, p. 3732-3740.

Blake, T.S., and Barley, M.E., 1992, T ectonic evolution of the late Arch aean to early Palaeoproterozoic Mount Bruce Megasequence Set, Western Australia: Tectonics, v. 11, p. 1415-1425.

Bluth, G.J.S., Schnetzler, C.C., Krueger, A.J., and Walter, L.S., 1993, The contribution of explosive volcanism to global atmospheric sulphur dioxide concentrations: Nature, v. 366, p. 327-329.

Habicht, K.S., Gade, M., Thamdrup, B., Berg, P., and Canfield D.E., 2002, Calibration of sulfate levels in the Archean ocean: Science, v. 298, p. 2372-2374.

Halevy, I., Johnston, D., and Schrag, D.P., 2010, Explaining the structure of the Archean mass-independent sulfur isotope record: Science, v. 329, p. 204-207.

Halmer, M.M., Schmincke, H.-U., and Graf, H.-F., 2002, The annual volcanic gas input into the atmosphere, in particular into the stratosphere: a global data set for the past 100 years: Journal of Volcanic and Geothermal Research, v. 115, p. 511-528.

Holland, H.D., 2002, Volcanic gases, black smokers, and the Great Oxidation Event: Geochimica et Cosmochimica Acta, v. 66, p. 3811-3826 (2002).

Kasting, J.F., Zahnle, K.J., Pinto, J.P., and Young, A.T., 1989, Sulfur, ultraviolet radiation, and the early evolution of life: Origin of Life and Evolution of the Biosphere, v. 19, p. 95-108.

Kellogg, W.W., Cadle, R.D., Allen, E.R., Lazrus, A.L., and Martell, E.E., 1972, The sulfur cycle: Science, v. 175, p. 587-596.

Krapež, B., Barley, M.E., and Pickard, A.L., 2003, Hydrothermal and resedimented origins of the precursor sediments to banded iron formations: sedimentological evidence from the early Palaeoproterozoic Brockman Supersequence of Western Australia: Sedimentology, v. 50, p. 979-1011.

Lambert, G., Le Cloarec, M.F., and Pennisi, M., 1988, Volcanic output of SO_2 and trace metals: A new approach: Geochimica et Cosmochimca Acta, v. 52, p. 39-42.

Leventhal, J.S., 1991, Comparison of organic geochemistry and metal enrichment in two black shales: Cambrian Alum Shale of Sweden and Devonian Chattanooga Shale of United States: Mineralium Deposita, v. 26, p. 104-112.

Pavlov, A.A., and Kasting, J.F., 2002, Mass-independent fractionation of sulfur isotopes in Archean sediments: strong evidence for an anoxic Archean atmosphere: Astrobiology, v. 2, p. 27-41.

Rasmussen, B., and Fletcher, I. R., 2010, Dating sedimentary rocks suing in situ U-Pb geochronology of syneruptive zircon in ash-fall tuffs < 1mm thick: Nature Geoscience, v. 38, p. 299-302.

Reinhard, C. T., Raiswell, R., Scott, C., Anbar, A. D., and Lyons, T. W., 2009, A Late Archean sulfidic sea stimulated by early oxidative weathering of the continents: Science, v. 326, p. 713-715.

Schieber, J., 2009, Discovery of agglutinated benthic foraminifera in Devonian black shales and their relevance for the redox state of ancient seas: Palaeoceanography, Palaeogeography, Palaeoecology, v. 271, p. 292-300.

Schieber, J., and Baird, G., 2001, On the origin and significance of pyrite spheres in Devonian black shales of North America: Journal of Sedimentary Research, v. 71, p. 155-166.

Simonson, B.M., Davies, D., and Hassler, S.W., 2000, Discovery of a layer of probable impact melt spherules in the Late Archaean Jeerinah Formation, Fortescue Group, Western Australia: Australian Journal of Earth Science, v. 47, p. 35-325.

Smith, R. E., Perdrix, J. L., Parks, T. C., 1982, Burial metamorphism in the Hamersley Basin, Western Australia: Journal of Petrology, v. 23, p. 75-102.

Zahnle, K.J., Claire, M., and Catling, D., 2006, The loss of mass-independent fractionation in sulfur due to a Paleoproterozoic collapse of atmospheric methane: Geobiology, v. 4, p. 271-283.

Table DR1.

FVG-1 (m)	TOC (wt. %)	Pyrite S (wt. %)	$\delta^{34}S$ (‰)	$\delta^{33}S$ (‰)	$\Delta^{33}S$ (‰)	Al (wt. %)	Mo (wt. %)	Total Fe (wt. %)	Acetate Fe (wt. %)	Dithionite Fe (wt. %)	Oxalate Fe (wt. %)	Pyrite Fe (wt. %)	Fe_{HR}/Fe_T	Fe_{PY}/Fe_{HR}	Fe_T/Al
748.3	1.8	0.9	1.2	1.37	0.27	8.4	2	6.6	0.3	0.3	0.7	0.7	0.3	0.4	0.8
749.65	3.3	2.7	2.2	1.96	0.42	8.6	2	4.7	0.3	0.2	1	2.3	0.8	0.6	0.5
750.56	6.1	1.2	0.9	0.99	-0.02	9	3	2.4	0.1	0.1	0.3	1	0.6	0.6	0.3
751.15	4.5	0.5	2.5	-	-	8.8	0	1.5	0.1	0.2	0.2	0.4	0.5	0.5	0.2
752.65	7.5	1.4	12.7	13.37	5.94	8.8	3	1.4	0.1	0.2	0.1	1.2	1.1	0.8	0.2
753.95	4.8	0.6	7.7	-	-	6	3	1.7	0.2	0.1	0.2	0.5	0.6	0.5	0.3
755.2	2.4	0.1	3.8	1.72	-0.47	2.9	1	2.2	0.4	0.1	0.6	0.1	0.6	0.1	0.8
756.6	3.8	0.3	8.6	2.04	0.16	5.4	1	1.4	0.4	0.1	0.1	0.3	0.6	0.3	0.3
756.8	5.6	0.7	4	1.66	-1.35	5.5	-	1.4	0	0.1	0	0.6	0.5	0.9	0.3
760.7	7.6	2	3.3	1.72	-0.47	7.3	2	2.4	0	0.1	0	1.7	0.8	0.9	0.3
761.8	5.9	3.6	2.6	2.86	1.08	6.2	3	3.9	0	0	0	3	0.8	1	0.6
764.45	4.6	1.7	2.3	0.77	-0.82	6.1	-	3.7	0.1	0	0	1.4	0.4	0.9	0.6
765	10.7	1.9	6	9.52	6.76	5.5	3	2.7	0.4	0.2	0.1	1.6	0.8	0.7	0.5
767.6	4.6	1.6	5	5.91	2.58	4.5	2	2.1	0.1	0	0.1	1.3	0.7	0.8	0.5
774	4.4	3.4	1.7	0.74	-0.73	5.7	3	4.5	0.2	0.1	0.1	2.9	0.7	0.9	0.8
775.55	4.7	2	3.3	1.6	-0.43	6	2	2.5	0.1	0.1	0.1	1.7	0.8	0.8	0.4
776.4	5.8	3	5.6	5.72	2.5	6.2	4	3	0.2	0.1	0.1	2.5	1	0.9	0.5
777.8	11.3	3.5	-0.7	1.07	1.04	5.8	3	3	0	0.1	0	3	1	1	0.5
779.45	10.1	3.3	0.2	2.24	1.87	5.8	2	3	0	0.1	0	2.7	1	0.9	0.5
780.3	1.2	0.5	-0.1	2.06	1.9	9	1	4	2	0.1	0.7	0.4	0.8	0.1	0.4
780.95	10	2.3	8.9	13.33	7.94	7.2	3	2.5	0.2	0.2	0.1	1.9	0.9	0.8	0.3
782.9	7.8	3.8	10.2	13.1	7.17	6.1	-	3.1	0.2	0.1	0.1	3.2	1.1	0.9	0.5
787.4	7.6	3.8	6.5	9.33	5.69	6.4	6	4.5	0.7	0.1	0.1	3.2	0.9	0.8	0.7
791	4.7	1.1	-0.4	-	-	7.7	4	3.6	0.6	0.1	0.3	0.9	0.5	0.5	0.5
794.1	4.7	2.9	1.7	6.4	4.82	6.7	4	5	0.2	0.1	0.3	2.4	0.6	0.8	0.8

796.2	4.4	0.8	1.1	-	-	7.1	4	4.5	1	0.1	0.8	0.7	0.5	0.3	0.6
797.05	4	1.1	7.5	11.3	6.98	7.9	6	4.5	0.3	0.1	0.7	0.9	0.4	0.5	0.6
802.1	1.7	0.5	3.5	-	-	5.6	3	5.1	0.4	0.2	0.6	0.4	0.3	0.3	0.9
813.25	1.5	0.2	1.5	-	-	6.3	-	4.1	2.5	0.2	0.4	0.2	0.8	0.1	0.7
813.6	2.5	0.8	3.7	-	-	6.4	3	4.3	0.2	0.1	0.9	0.7	0.5	0.3	0.7
815.2	2.7	0.5	2.4	5.06	3.44	7.7	4	4.9	0.5	0.1	0.9	0.4	0.4	0.2	0.6
818.8	2.2	0.2	2.5	-	-	7.4	4	5.2	0.6	0.1	0.6	0.2	0.3	0.1	0.7
822.45	2.3	0.8	0.2	1.56	1.19	5.8	3	4.7	0.7	0.1	1.1	0.6	0.5	0.2	0.8
823.3	3.4	0.5	2.8	-	-	6.6	3	4.5	0.3	0.1	0.2	0.4	0.2	0.4	0.7
829.9	2.3	0.6	2.6	4.33	2.65	6.8	5	5.1	1.2	0.2	0.4	0.5	0.5	0.2	0.8
849.6	1.4	0.5	0	-	-	6.7	-	4.7	0.2	0.1	0.1	0.4	0.2	0.5	0.7
855.65	0.7	0.8	-0.3	-	-	7.8	3	7.5	1.1	0.1	0.4	0.7	0.3	0.3	1
861.05	0.9	0.4	-0.7	-	-	8.4	2	5.8	0.4	0.1	1.1	0.4	0.3	0.2	0.7
881.7	1.5	0.4	1.3	-	-	8.3	2	4.8	0.2	0.1	1.1	0.3	0.4	0.2	0.6